Analysis of a Generic T-Tail Transport using a Surface-Vorticity Panel Method Flow Solver at Low Angles of Attack

Cade M. May*
Auburn University, Auburn, Alabama, 36830

A panel method flow solver with viscous capabilities was used to determine aerodynamic coefficients and dynamic stability derivatives of a well-studied generic T-tail (GTT) transport aircraft model. Dynamic stability derivatives were computed using two different solver modes within the FlightStream® panel method flow solver, the pseudo-steady state and unsteady state solvers. The unsteady solver results were computed using the forced oscillation (F-O) method and post-processed using an integration method. Solver results were compared with experimental data and USM3D flow solver data. Both solver modes agree with published data in sign and relative magnitude. The pseudo-steady state solver performed similarly to the USM3D flow solver in certain cases. The solver did not correctly capture the same trends seen in experimental data in every case, but the data support the use of the tool as a rapid preliminary design and analysis tool for approximate results. The effects of using 1, 2, and 3 total forced oscillation cycles on the unsteady solver precision were also studied, with the results showing that the unsteady solver produced similar data at all numbers of cycles used with the forced oscillation method. The advantages of using the solver in finding dynamic stability parameters include low computational cost, significantly reduced computation times, and the requirement of only surface meshes. The main disadvantage is a trade-off in accuracy for the faster solver. Future work should focus on the ability of the solver to handle control surface deflection within the pseudo-steady and unsteady state solver modes. The solver showed promising capabilities in rapidly calculating approximate dynamic stability derivatives, supporting its use in the preliminary design process.

Nomenclature

A	=	forced oscillation amplitude (deg)
b	=	wingspan (ft)
$\bar{c}$	=	mean aerodynamic chord (ft)
C_D	=	drag coefficient
C_L	=	lift coefficient
C_M	=	moment coefficient
$C_{l,p}$	=	roll damping coefficient
$C_{m,q}$	=	pitch damping coefficient
$C_{n,r}$	=	yaw damping coefficient
d	=	fuselage diameter (ft)
f	=	frequency (Hz)
k_P	=	reduced frequency for pitch oscillation
k_R	=	reduced frequency for roll oscillation
k_Y	=	reduced frequency for yaw oscillation
M_∞	=	freestream Mach number
MRC	=	Moment Reference Center (ft)
$\bar{q}$	=	dynamic pressure, (lb/ft^2)
Re	=	Reynolds number
s	=	wing reference area (ft^2)
t	=	time (s)

*Undergraduate, Department of Aerospace Engineering, Auburn AL, Student Member 1603387.

t_o = starting time (s)
T = total period of forced oscillation motion (s)
u_∞ = freestream velocity (ft/s)
α = angle of attack (deg)
ω = forced oscillation frequency (s^{-1})

Key Acronyms

12-Ft LST = NASA Langley Research Center 12-Foot Low-Speed Tunnel
CFD = Computational Fluid Dynamics
F-O = Forced Oscillation
FVWT = Boeing Flow Visualization Water Tunnel
GTT = Generic T-Tail
NAART = Boeing North American Aviation Research Tunnel
SA = Spalart-Allmaras one-equation turbulence model
SCT = Stability and Control Toolbox
SST = Menter Shear Stress Transport two-equation turbulence model

I. Introduction

Obtaining dynamic stability derivatives is a crucial aspect of aircraft design. Physically running experiments to obtain dynamic stability derivatives can be costly [1], so engineers naturally turn towards computational fluid dynamics (CFD) simulations to save time and effort. However, CFD methods can struggle with precision and reliability when finding dynamic stability characteristics. High-approximation CFD tools, which attempt to reduce computational requirements and save time, have also previously struggled to obtain even vaguely similar results to experimental data [1]. Determining dynamic stability derivatives is costly, time-consuming, and/or computationally intensive. Thus, developing new methods to compute these aerodynamic coefficients more rapidly and at lower cost remains a high priority for researchers.

One such method examined is the panel-method flow solver. Although it is not likely that a panel method flow solver could replace all 3-D CFD tools in finding dynamic stability derivatives, validating such a flow solver in specific applications could be quite valuable at specific points in the aircraft design process. One of these applications, aircraft loss of control, is a crucial area of research in aviation safety. The performance of aircraft near stalling speed is studied experimentally and computationally to increase the accuracy of pilot training models in civil aviation. In response to aircraft loss of control accidents, the Federal Aviation Administration enacted new regulations in 2014 requiring pilots to undergo recovery from stall and upset training [2]. As a result, NASA and Boeing Research and Technology partnered to analyze the near-stall characteristics of a generic T-tail (GTT) transport aircraft using wind-tunnel tests, water-tunnel tests, and CFD simulations [3]. Using the results of these methods, a flight simulator model was even developed to advance the field of pilot stall training [4]. This GTT model has been studied extensively near the stalling speed both computationally and through physical testing. Vast amounts of stability data from various experimental methods are available on this model, making it an ideal choice for validation work of any panel method flow solver.

This paper focuses on the FlightStream® panel method flow solver. The solver was developed with surface vorticity, compressible flow, and viscous capabilities in an effort to provide quick, inexpensive, and accurate analysis of aerodynamic designs. In this work, the GTT model was analyzed using the solver and compared to published wind tunnel, water tunnel, and 3-D CFD data of the same design to understand the accuracy of the flow solver in computing dynamic stability derivatives.

II. Model Geometry

The generic T-tail (GTT) geometry used in this work was derived from a remotely controlled aircraft developed by NASA and Area-I, Inc. [5]. This scaled-model aircraft was intended for use by NASA in loss-of-control prevention research but ultimately was never flown to this end. Further research by NASA and Boeing utilized a slightly altered form of this aircraft in ground tests and simulations. This altered aircraft model is the GTT plane on which this work

is based and is intended to mimic the common form of regional civilian transport with a T-tail and aft twin-engine configuration.

The full-scale design characteristics of the GTT aircraft are shown in Table 1. More specific drawings of the GTT model showing various design parameters can be found in Ref. [6]. The moment reference center (MRC) was placed at 25% of the mean aerodynamic chord location. The engines were modeled as flow-through nacelles, and the main wing airfoil was modeled as a NASA SC(2)-0714 airfoil.

Table 1 GTT Full-Scale Reference Parameters

Aerodynamic Reference	Symbol	Value
Wingspan	b	75.98 ft
Mean Aerodynamic Chord	$\bar{c}$	11.07 ft
Fuselage Diameter	d	8.356 ft
Wing Area	s	754.32 ft^2

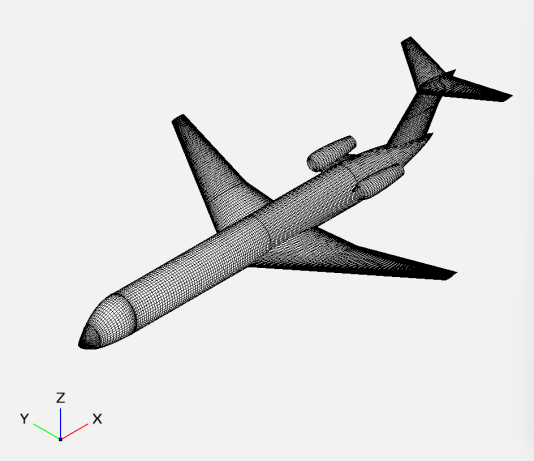

(a) Left Isometric View

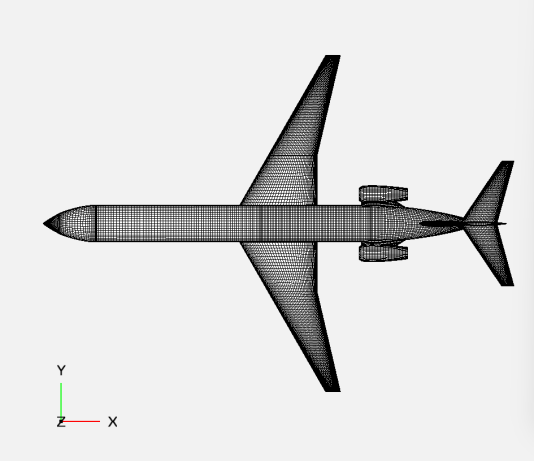

(b) Top View

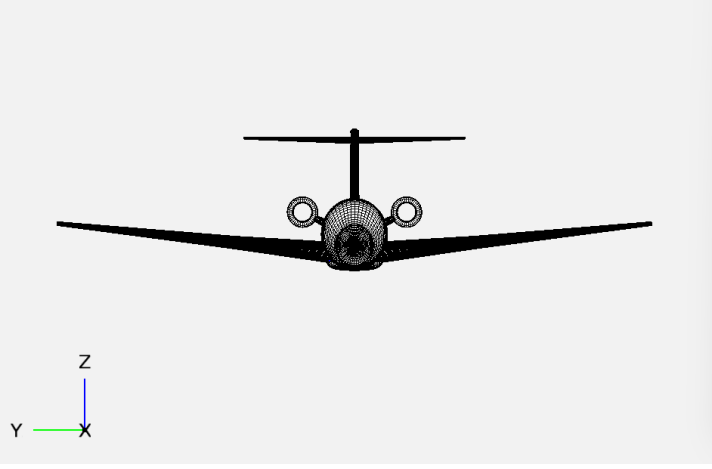

(c) Front View

Fig. 1 OpenVSP GTT Aircraft Mesh Angles

III. Computational Setup

A. Subsonic Panel Method Flow Solver

The solver is a surface vorticity panel method that combines compressible and viscous capabilities in a highly efficient way. The efficient design of the solver enables the user to generate rapid analysis of both conventional and unconventional aircraft with a unique analysis capability derived from surface vorticity, flow-separation, and viscous effects applicable to both powered and unpowered configurations. Loads are successfully predicted using surface vorticity on an unstructured surface mesh with the attached flow, and aerodynamic loads are computed by shedding vorticity from the analyzed geometry [7].

The solver uses three main boundary layer models for viscous analysis: laminar, turbulent, and transitional. All three models are two-dimensional, modified and implemented along on-body surface streamlines. The solver can model complex separation physics along streamlines as a result of including the transitional boundary layer model [7].

The unsteady time-domain solver mode is used for time-varying simulations. The unsteady solver requires an arbitrary motion definition included by the user, which can include a position map in a given coordinate direction, among many other possibilities. The wake system within the unsteady solver is a full unsteady, time-evolving relaxed vortex filament wake model.

Simulation run times are measured in terms of minutes because of the formulation of the solver. The panel method shows promising capabilities in rapidly analyzing geometries at any point in the design process.

B. Grid Setup

Modeling the GTT only required developing a surface mesh because the solver is a panel method. As such, the characteristics of the GTT surface grid only will be described here. The GTT surface grid was modeled using OpenVSP, an open-source parametric aircraft geometry tool developed by NASA and released to the public domain in 2012. The GTT file was then converted into a Plot3D file and exported to the solver, where it was further refined using pre-processing tools within the solver. This produced a hybrid structured-unstructured grid format comprised of quadrilateral panels everywhere except for triangle panels where components intersected. After all mesh processing, the total number of panels in the GTT simulation was 79,164.

C. Boundary Conditions

The free-stream velocity was set to u_∞ = 140.7 ft/s for a Mach number of M_∞ = 0.126 at sea-level conditions. The viscosity was changed to achieve a Reynolds number consistent with reference data. The corresponding fluid properties used in all simulations are summarized in Table-2 below. Trailing-edge wake boundary conditions were marked at the rear of all lifting surfaces (i.e., the main wings, horizontal and vertical stabilizers, engines, and engine pylons). Wake termination locations were set at the intersections of these trailing edges with any other bodies according to the standard best practices for the solver.

Table 2 Freestream Flow Properties

Property	Value
Density	1.225 kg/m^3
Mach Number	0.126
Pressure	101324.02 Pa
Ratio of Specific Heats	1.400
Reynolds Number	1.600 million
Sonic Velocity	340.29 m/s
Temperature	288.17 K
Viscosity	0.0001108 Pa-s

The pseudo-steady state and unsteady solver modes within the solver were used to find dynamic stability derivatives. The steady-state solver was utilized to compute all static aerodynamic coefficients. The unsteady solver requires the definition of a custom motion, which was defined according to the referenced forced oscillation (F-O) data processing

and analysis method [8]. 3 total custom motions were made, with each corresponding to one of three dynamic stability derivatives found in this work. Each custom motion can be used at any angle of attack within the solver. The custom motions were each an angular position map constructed using pre-determined amplitude and frequency values along the X, Y, or Z axis containing 3 complete periods of oscillation. Defining the motions for 3 periods of oscillation increased computational time but was done to minimize errors in computations. The amplitude and reduced frequency values for each of the 3 custom motions depended on the dynamic stability derivative being computed and are summarized in Table 3. These values were obtained from Ref. [9]. All forced oscillation angular position maps were formed using the frequency value obtained from the reduced frequency value using basic algebra.

Table 3 Unsteady Custom Motion Definitions for Each Dynamic Derivative

	$C_{l,p}$	$C_{m,q}$	$C_{n,r}$
Amplitude of Oscillation	± 10°	± 5°	± 10°
Axis of Rotation	X	Y	Z
Custom Motion Reduced Frequency Variable	k_R	k_P	k_Y
Custom Motion Reduced Frequency Definition	$\pi f b/u_\infty$	$\pi f \bar{c}/u_\infty$	$\pi f b/u_\infty$
Custom Motion Reduced Frequency Value	0.094	0.0158	0.094

The pseudo-steady state solver mode, found within the Stability and Control Toolbox (SCT) of the solver, requires the definition of coefficients. The numerator parameter of each dynamic stability derivative was set to the moment about the corresponding axis of rotation, and the denominator parameter was set to the angular rate about the corresponding axis of rotation. The geometry boundaries included the entire mesh, and the coordinate system used was the reference coordinate system. The angular rate increment was set to 0.2000 rad/s in all simulations. The coefficient constants used in all pseudo-steady state simulations are summarized in Table 4 below.

Table 4 Pseudo-Steady State Solver Coefficient Constants

	$C_{l,p}$	$C_{m,q}$	$C_{n,r}$
Coefficient Definition	$2u_\infty \bar{c}/b^2$	$2u_\infty/\bar{c}$	$2u_\infty \bar{c}/b^2$
Coefficient Value	0.5396	25.4201	0.5396

D. Solver Settings

In this study, three different solver modes were utilized: steady, pseudo-steady, and unsteady states. In all solver modes, a turbulent viscous boundary layer was simulated with a surface roughness height of 0 nm, assuming a smooth surface. Viscous coupling was enabled, with the fuselage excluded to save time in the computation. Flow separation was enabled; all surfaces containing a trailing edge were set to axial separation and the remaining surface (i.e., the fuselage) was set to crossflow separation. The coefficient for crossflow separation was set to −0.6950, corresponding to the fuselage diameter. Induced drag was calculated from a vorticity-based drag model for bodies with trailing edges and calculated from a pressure-based drag model for the fuselage. All simulations used a maximum number of iterations of 500 and a convergence threshold of 1e-5. The freestream reference values used throughout this study can be found in Table 2, and the coefficients used in the pseudo-steady state solver can again be found in Table 4.

For the unsteady solver mode, the unsteady pressure and Kutta terms checkbox found within the advanced settings of the solver was enabled. The number of time steps and total time used for each dynamic stability derivative are summarized in Table 5 below. These values were obtained from the forced oscillation method described in the Boundary Conditions section of this paper and in Ref. [8]. Each unsteady time step increment was set to 0.1000 seconds.

Table 5 Unsteady Time Settings for each Dynamic Stability Derivative

	$C_{l,p}$	$C_{m,q}$	$C_{n,r}$
Number of Time Steps	543	471	543
Total Time	54.3 sec	47.1 sec	54.3 sec

E. Performance

These results were obtained from a desktop computer having two Intel Xeon processors with fifty-six total threads and twenty-eight physical cores. Only twelve parallel threads were allowed at once. The complete panel of aerodynamic coefficient solutions was obtained in ≈ 30 minutes. The pseudo-steady state solver simulation took ≈ 4.5 minutes to run at each angle of attack; all data for each dynamic stability derivative was found in ≈ 27 minutes. Each unsteady time step took ≈ 2 minutes to compute, totaling ≈ 17 hours for 3 oscillatory cycles.

IV. Data Post-Processing

Obtaining the dynamic stability derivatives from the unsteady solver required post-processing of the data. Specifically, an integration method was used that was derived from the defining parameters of the forced oscillation method. Equations 1 through 3 were used to calculate the pitch, roll, and yaw damping coefficients, respectively. These equations were obtained from Ref. [8], where detailed derivations can be found. The values for frequency, amplitude, and period came from the forced oscillation motion parameters. The integration was performed by multiplying the unsteady solver force results by the cosine of the forced oscillation frequency multiplied by the time at each time step and then applying the trapezoidal integration rule to the results. This value was then multiplied by the constant outside of the integral, which gave the dynamic stability derivative at a specific angle of attack. This was repeated a total of 18 times to obtain all unsteady solver data for this study.

$$C_{m,q} = \frac{4u_\infty}{\bar{q}s\bar{c}^2\omega AT}\int_{t_0}^{t_0+T}[M_b(t) - M_i(t)]\cos(\omega t)\,dt \tag{1}$$

$$C_{l,p} = \frac{4u_\infty}{\bar{q}sb^2\omega AT}\int_{t_0}^{t_0+T}[L_b(t) - L_i(t)]\cos(\omega t)\,dt \tag{2}$$

$$C_{n,r} = \frac{4u_\infty}{\bar{q}sb^2\omega AT}\int_{t_0}^{t_0+T}[N_b(t) - N_i(t)]\cos(\omega t)\,dt \tag{3}$$

V. Results

Aerodynamic coefficients and dynamic stability coefficients were calculated using 3 flow solver modes available in FlightStream®. These results were then compared with data previously obtained from wind tunnel tests, water tunnel tests, and USM3D, a widely used 3-D flow solver. All tests and simulations were performed at low Reynolds numbers measured at the mean reference center. First, the static stability solutions will be discussed. Then the dynamic stability solutions will be discussed, followed by a look at the precision of the unsteady flow solver mode with less forced oscillation cycles. The focus of these results should be on the performance of the panel method flow solver in comparison to 3-D simulation runs and physical testing.

A. Static Stability Solutions

Before the dynamic stability derivatives were computed, the aerodynamic coefficients were found to validate the accuracy of the setup. Figure 2 shows the results of the static stability simulation runs against the GTT reference data at angles of attacks between 0- and 12-degrees. The Reynolds number of all data sources in the figures was 1.6 million. Data obtained from the solver is in good agreement with the published data [9] at low angles of attack. The lift and moment characteristics predicted by the solver fall within or close to the values of the reference data. The solver predicts the stall region beginning around a 9-degree angle of attack, which notably is in good agreement with wind tunnel results. The drag values predicted by the solver fall slightly below the reference data up until the 9-degree angle of attack, though the trend is similar to all other data sources. After a 9-degree angle of attack, the drag values found by the

solver diverge from the reference data. This divergence in drag values made it clear that the scope of the study moving forward should be on the performance of the GTT at low angles of attack (i.e., roughly 10 degrees or less).

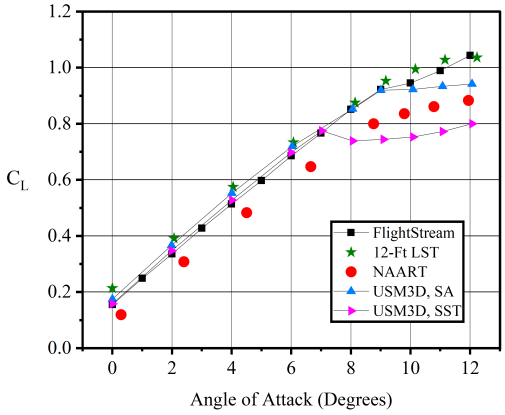

(a) C_L **vs.** α

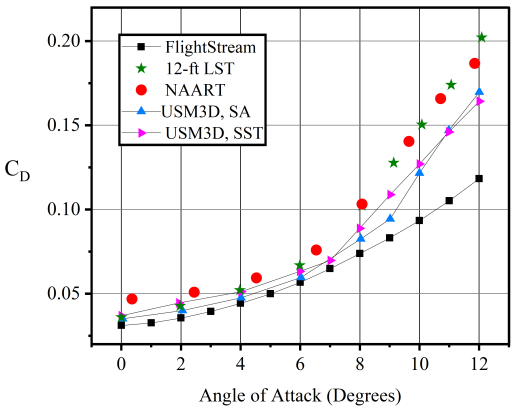

(b) C_D **vs.** α

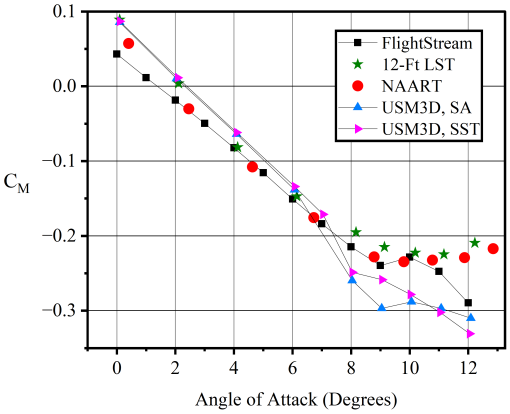

(c) C_M **vs.** α

Fig. 2 Aerodynamic Coefficient Solutions, Re = 1.6 Million

B. Dynamic Stability Solutions

The dynamic stability solutions are presented in Fig. 3. All solver simulations were run at a Reynolds number of 1.6 million, and the USM3D comparison data followed the Spalart-Allmaras (SA) one-equation turbulence model. All dynamic stability derivatives are per radian. For the 3 coefficients examined, both solver modes tested within the solver produced the correct sign (i.e., negative) as well as magnitudes similar to the comparison data [6][9]. Variance was found between trends and the precise magnitude of each data point.

For the pitch damping coefficient ($C_{m,q}$), the unsteady solver mode predicted magnitudes higher than all other data sources while the pseudo-steady state solver mode predicted magnitudes lower than all other data sources. The pseudo-steady state solver mode data is closest in value to the USM3D results, though it is unclear if the USM3D data point at an 8-degree angle of attack is an outlier. Without this point included in the USM3D data series, the pseudo-steady state solver mode predicts results remarkably like those predicted by the USM3D solver. However, it should be noted that the USM3D solver was only used to produce 2 data points within the range of the solver simulation runs (0- to 10-degree angle of attack). More complete data from USM3D would provide a clearer comparison between the two CFD software.

For the roll damping coefficient ($C_{l,p}$), both the unsteady and pseudo-steady state solver modes predicted magnitudes

lower than the other data up to an 8-degree angle of attack. While the unsteady solver mode did not demonstrate the same sensitivity to increasing angle of attack that the other data show (except for the water tunnel), the pseudo-steady state solver mode was able to capture the same trend of decreasing magnitude of coefficient value past an 6-degree angle of attack shown by the other data. It is important to note that the flow solver modes were operated at a Reynolds number of 1.6 million in every simulation run, which varied from the USM3D simulation runs for $C_{l,p}$. It would be ideal for all data sources to be run at the same Reynolds number; simulating the flow with different Reynolds numbers could have affected the magnitude and trend of the resultant values for the CFD comparison.

For the yaw damping coefficient ($C_{n,r}$), the unsteady and pseudo-steady state flow solver modes predicted magnitudes lower than all data sources. The exception is the USM3D flow solver at an 8-degree angle of attack versus the pseudo-steady state flow solver. The other data sources were in less agreement for the yaw damping coefficient than they were for the other 2 damping coefficients. This makes a comparison with specific trends difficult, though the two solver modes tested were close in agreement with each other to this end. The water tunnel was only tested at 3 points between a 0- and 10-degree angle of attack, while the USM3D solver was only run at 2 points in the same range. More comprehensive comparison data in this range would benefit this study.

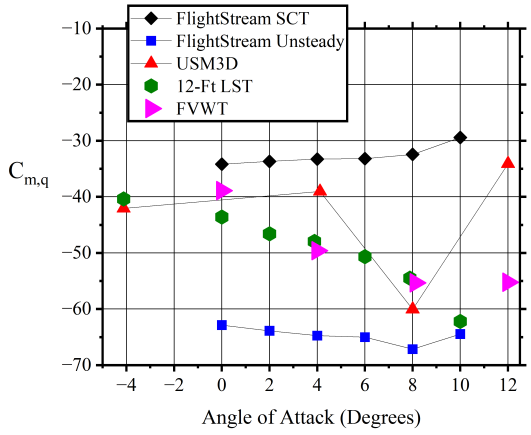

(a) $C_{m,q}$ **vs.** α

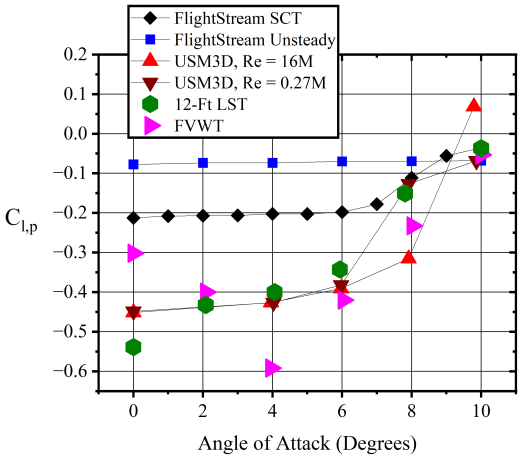

(b) $C_{l,p}$ **vs.** α

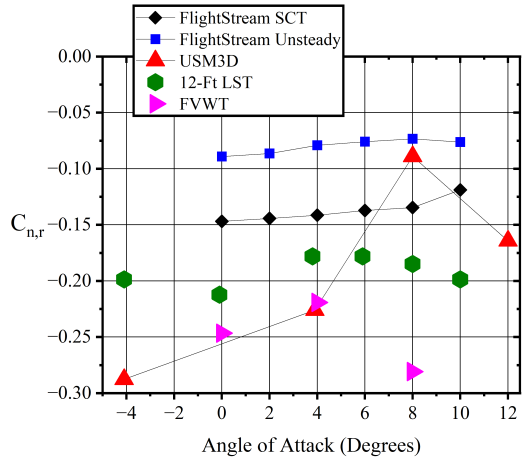

(c) $C_{n,r}$ **vs.** α

Fig. 3 Dynamic Stability Coefficient Solutions

C. Forced Oscillation Cycles

For comparison against published data up to this point, the unsteady solver results within the solver were post-processed using the results from 3 complete forced oscillation cycles. However, time could be saved in computation within the solver by simulating only one or two cycles. To investigate how using fewer cycles impacts the final result, the data was post-processed using one and two forced oscillation cycles. Figure 4 shows the comparison of each dynamic stability derivative at all angles of attacks used to compute data in this work for 1, 2, and 3 complete forced oscillation cycles. Tables [6-8] show the percentage differences between both 1 and 2 forced oscillation cycles versus 3 forced oscillation cycles at each angle of attack for each dynamic stability derivative. The maximum percentage difference for all values was 4.013%, which was found at an 8-degree angle of attack for the 1 forced oscillation cycle used to compute $C_{m,q}$. $C_{l,p}$ showed no percentage differences higher than 1.793%, and $C_{n,r}$ showed no percentage differences higher than 1.143%. Considering the amount of time that using even one less forced oscillation cycle in the unsteady solver mode can save, these percentage differences can be considered relatively small. These results show that the unsteady solver mode could serve a useful purpose in preliminary design and analysis, especially as a means to validate the results of the pseudo-steady state solver mode.

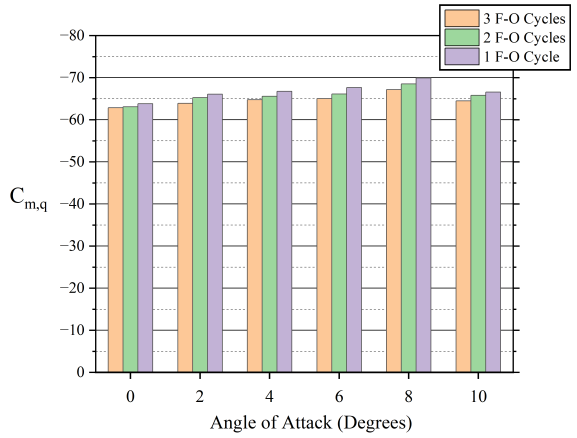

(a) $C_{m,q}$

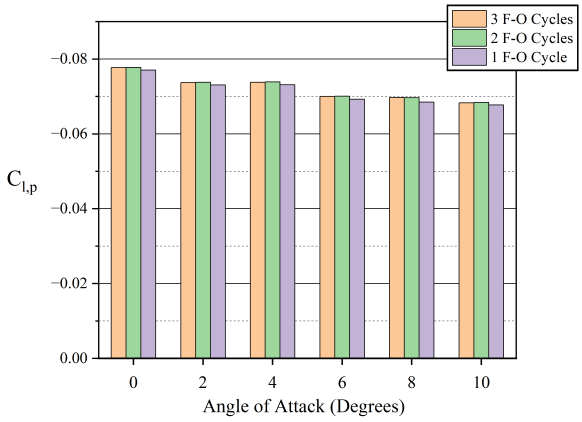

(b) $C_{l,p}$

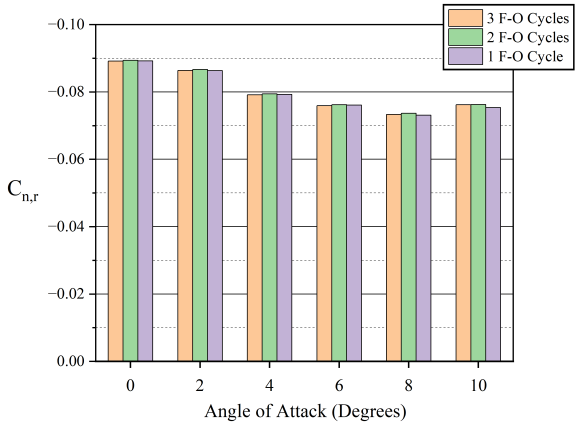

(c) $C_{n,r}$

Fig. 4 Forced Oscillation Cycle Comparison for Dynamic Stability Coefficients

Table 6 $C_{l,p}$ **F-O Cycle Percentage Differences from 3 Cycles Based on Angle of Attack**

AoA (deg)	2 Cycles % Difference	1 Cycle % Difference
0	0.123	0.820
2	0.130	0.846
4	0.113	0.925
6	0.077	1.083
8	0.095	1.793
10	0.180	0.822

Table 7 $C_{m,q}$ **F-O Cycle Percentage Differences from 3 Cycles Based on Angle of Attack**

AoA (deg)	2 Cycles % Difference	1 Cycle % Difference
0	0.362	1.484
2	2.081	3.334
4	1.258	3.047
6	1.698	3.947
8	1.980	4.013
10	2.048	3.201

Table 8 $C_{n,r}$ **F-O Cycle Percentage Differences from 3 Cycles Based on Angle of Attack**

AoA (deg)	2 Cycles % Difference	1 Cycle % Difference
0	0.305	0.067
2	0.287	0.100
4	0.315	0.112
6	0.342	0.174
8	0.445	0.282
10	0.072	1.143

VI. Conclusions

The FlightStream® panel method flow solver was used to determine the dynamic stability derivatives of a widely examined aircraft model. The dynamic stability derivatives near the stalling speed of a generic T-tail (GTT) transport model, including pitch, yaw, and roll damping coefficients, were calculated within the unsteady and pseudo-steady state solver modes of the solver and compared with published data. Aerodynamic coefficients were found to determine the accuracy of the GTT reconstruction and to determine the angle of attack range for computations. The dynamic solutions were accordingly found between a 0- and 10-degree angle of attack.

The results of the solver modes agree in sign and relative magnitude with the published data. The pseudo-steady state solver mode was overall more accurate than the unsteady solver mode, and it even produced data similar to the comparison 3-D flow solver for the pitch damping coefficient. The unsteady solver mode, which relied on data post-processing via the forced oscillation method, was found to retain precision with lower amounts of total cycles.

The advantages of the solver in computing dynamic stability derivatives include low computational cost, significantly reduced computation times, and the need only for a surface mesh. Disadvantages include lower accuracy than the comparison 3-D solver when compared to wind tunnel and water tunnel data, lack of precise agreement in magnitude between solver modes, and inconsistent similarity with the trends of physical testing data. This study would benefit from more comprehensive data within the angle of attack range concentrated on in this work. Future work should focus on the effects of control surface deflection on solver results.

The results of both solver modes support the use of the solver as a rapid preliminary design and analysis tool in the computation of dynamic stability derivatives at low angles of attack.

References

[1] Lawrence Green, Angela Spence and Patrick Murphy. "Computational Methods for Dynamic Stability and Control Derivatives," AIAA 2004-15. 42nd AIAA Aerospace Sciences Meeting and Exhibit. January 2004.

[2] “Qualification, Service, and Use of Crewmembers and Aircraft Dispatchers; Final Rule, 14 CFR Part 121,” Federal Aviation Administration, Federal Register, Vol 78, No. 218, Nov. 12, 2013, 2013. URL: http://www.gpo.gov/fdsys/pkg/FR-2013-11-12/pdf/2013-26845.pdf.

[3] Cunningham, K., Murphy, P. C., Gautam H. Shah, M. A. H., and Pickering, B. P., “Flight Dynamics Modeling for Stall Training,” 57th AIAA Aerospace Sciences Meeting, AIAA, 2019.

[4] Cunningham, K., Shah, G. H., Hill, M. A., Pickering, B. P., Litt, J. S., and Norin, S., "A Generic T-tail Transport Airplane Simulation for High-Angle-of-Attack Dynamics Modeling Investigations," 2018 AIAA Modeling and Simulation Technologies Conference, AIAA, 2018. https://doi.org/doi:10.2514/6.2018-1168

[5] Daniel Kuehme, Nicholas R. Alley, Caleb Phillips and Bruce R. Cogan. "Flight Test Evaluation and System Identification of the Area-I Prototype-Technology-Evaluation Research Aircraft (PTERA)," AIAA 2014-2577. AIAA Flight Testing Conference. June 2014.

[6] Cunningham, K., et al., “Preliminary Test Results for Stability and Control Characteristics of a Generic T-tail Transport Airplane at High Angle of Attack”, Submitted for Publication AIAA Atmospheric Flight Mechanics Conference , AIAA SciTech Forum, January, 2018.

[7] Burkhalter, J. E., Ahuja, V., Hartfield R., “Robust prediction of high lift using surface vorticity”, NASA SBIR NNX17CL12C, Phase II final report, 2017.

[8] Vicroy, Dan, "A Guide to Forced Oscillation Data Processing and Analysis", NASA 20210023569. https://ntrs.nasa.gov/citations/20210023569

[9] Susan N. McMillin, Neal T. Frink, Patrick C. Murphy, Kevin Cunningham, Gautam H. Shah and Sudheer N. Nayani. "Computational Study of a Generic T-tail Transport," AIAA 2019-0036. AIAA Scitech 2019 Forum. January 2019.